A dual-phase-lag (DPL) transient non-Fourier heat transfer analysis of functional graded cylindrical material under axial heat flux

M. Hadi Ghasemi[1], S. Hoseinzadeh[2,*], S. Memon[3,*]

[1] Department of Mechanical Engineering, West Tehran Branch, Islamic Azad University, Tehran, Iran.

[2] Department of Planning, Design, and Technology of Architecture, Sapienza University of Rome, Piazzale Aldo Moro, 5, 00185 Roma RM, Italy.

[3] Solar Thermal Vacuum Engineering Research Group, London Centre for Energy Engineering, School of Engineering, London South Bank University, London SE1 0AA, UK.

[*]Correspondence: SM: S.Memon@lsbu.ac.uk; SH: siamak.hosseinzadeh@uniroma1.it

[*]Corresponding Author: Saim Memon

Address: Solar Thermal Vacuum Engineering Research Group, London Centre for Energy Engineering, School of Engineering, London South Bank University, London SE1 0AA, UK.

Official Website: https://www.lsbu.ac.uk/about-us/people/people-finder/dr-saim-memon

Google Scholar: https://scholar.google.co.uk/citations?user=Smt5s-IAAAAJ&hl=en

ORCID: https://orcid.org/0000-0003-2598-8935

Abstract

A dynamic thermal conduction problem needs a mathematical formulation and solution consisting of cylindrical coordinates of materials for the application of nuclear reactor and/or laser therapeutic when subjected to higher heat fluxes. In this study, dual-phase-lag (DPL) transient non-Fourier heat conduction in a functional graded cylindrical material is analytically solved under axial heat flux condition. Functional Graded Material (FGM) properties are based by exponential low. Governing equations on the model are expressed in 2D cylindrical coordinates and solved by using the separation of variable method. . An effect of the heterogeneity coefficient of the material using Fourier method, Cattaneo–Vernote model and the dual phase lag is analyzed. An influence of non-dimensional temperature changes to the Fourier number in the pure and functional material is analyzed. Results showed that DPL model requires less time to meet the steady temperature compared with single-phase-lag (SPL) model. In the FGMs, each model and method tends to have a constant temperature based on the amount of heterogeneity coefficient, and it can be concluded that one of the factors determining the amount of stable temperature is the properties of the material. The current results provide a straightforward multivariate analytical solution of the non-Fourier conduction equation in a finite cylinder, for cylinders with any boundary conditions and, for cylinders with functional graded materials. It was found that negligible issues with the critical points being presented when compared to the Laplace operator method.

Keywords: dual-phase-lag, non-Fourier heat conduction, Functional graded materials, Axial heat flux.

Nomenclature			
ρ	Density	Fo	Dimensionless time (Fourier number)
c	Specific heat [$Jkg^{-1}K^{-1}$]	θ	Dimensionless temperature
T	Temperature [K]	α_0	Thermal diffusivity [m^2s^{-1}]
T_∞	Surrounding temperature [K]	ω	Dimensionless height
t	Time [s]	Ve_T	Dimensionless phase lag of the temperature gradient (Vernote number)
r	Radial coordinate [m]	Ve_q	Dimensionless phase lag of the heat flux (Vernote number)
z	Height coordinate [m]	M	Length to radius ratio of the cylinder
K	Thermal conductivity [$Wm^{-1}K^{-1}$]	q_0	heat flux [Wm^{-2}]
τ_T	Phase lag of the temperature gradient [s]	β	FG parameter
τ_q	Phase lag of the heat flux [s]	ψ	Transient solution
R	Radius of the cylinder [m]	ϕ	Steady solution
L	The length of the cylinder [m]	J_A	Bessel Function of first kind and order A
ξ	Dimensionless radius	Y_A	Bessel Function of second kind and order A

1. Introduction

It is necessary to establish a mathematical formulation and solution of the complex thermal conductivity equations having cylindrical coordinates of materials for the application of nuclear reactors, laser therapeutic and industrial engineering which are subjected to higher temperature environments. These materials are non-homogenous in its structure having smooth and consistent spatial variance in their thermo-mechanical properties because of the gradual shift in their microstructures under dynamic temperatures. The notion of gradual structure for composites and polymeric materials was first introduced in 1972 by Shen and Bever [1]. To achieve a graduated shape, various models for modifying the composite and polymerization were used. In which, functional graded materials (FGM) are found to be have dynamic microscopic structure due to their gradual change in volume fraction of the constituent materials and the mechanical microscopic model of the functional material, which are based on the fractional volume-shape approximation of the phase dispersion [2].

A number of analytical solutions are developed such as Wang etal [3] proposed an analytical solution by separating the variables for the hyperbolic equation, as well as a dual-phase-lag with the boundary condition of dirichlet, Neumann, and Robin in one-dimensional finite region. They also suggested a solution procedure for the multidimensional case and investigated the presence and consistency of the solution in comparison to the initial conditions. Baumeister and Hamill [4] investigated temperature changes in a semi-infinite solid under the constant temperature boundary condition with a hyperbolic model. Maurer and Thompson [5] proposed an analytical solution to non-Fourier heat conduction problems under constant flux boundary conditions. Özisik and Vick [6] obtained the analytical solution of the hyperbolic conduction heat transfer equation, on the assumption of a wave nature to transfer heat energy in a finite sheet by producing internal energy and the insulation boundary condition. Moosaie [7] solved analytically hyperbolic two-dimensional heat transfer equations with an arbitrary initial condition and a homogeneous as well as

inhomogeneous type 1 boundary condition. Barletta and Pulvirenti [8] solved the unstable hyperbolic conductivity for a solid cylinder of infinite length under the time-dependent heat flux boundary condition. This analytical solution was performed by Laplace transform method and investigated two special modes of constant flux and exponential decreasing flux with time. Anbarloei and Shivanian [9] considered the conduction heat transfer coefficient as a function of temperature and the displacement heat transfer coefficient using the power law as a function of temperature on a fin, and presented an analytical solution. Amiri and Norouzi [10] worked on the heat transfer of a hollow composite sphere. They considered their composite as a layer and examined it under the various boundary conditions. They used the separation of variables (SOV) and the Laplace transform methods to solve the equations. Ghasemi et al [11] analytically solved dual-phase-lag Transient non-Fourier heat conduction in a solid cylinder for constant axial heat flux. It was demonstrated that the DLP (dual phase lag) model takes less time to reach steady temperature as compared to single phase lag and Fourier models. Askarizadeh and Ahmadikia [12] investigated the high degree of the DPL heat transfer with thermodynamic compatibility. They were able to show that the first and second order of dual phase lag in some environmental conditions correspond to the second law of thermodynamics. Li, Lei and Wen [13] investigated a two-dimensional nonlinear partial differential equation on the composite functional structure of a cylinder in comparison to both finite element and finite difference methods.

Yang etal [4] investigated DPL heat transfer in the wall of a cylindrical furnace of functional material. They considered the structure of the furnace functional materials based on the power law and simulated their equations based on the T-wave model. The heat transfer analysis of integrated conduction and radiation modes in a planar conducting-radiating medium was studied by C. Mishra and K. Chaurasia [15] using the lattice Boltzmann method and showed the effects of lag ratio, extinction coefficient, scattering albedo, and conduction-radiation parameter on transient temperature distributions. Akbarzadeh and Chen [16] solved the one-dimensional non-Fourier heat conduction equation based on the DPL in the coordinates of Cartesian, cylindrical and spheres of functional material. They simulated their equations using T-wave model and provided the basis for determining the properties of a functional graded material with the power law. Hosseini etal [17] solved the classical Fourier heat transfer in a hollow cylinder made of functional graded material. They continuously considered the properties of the FGM according to the power law and solved heat transfer equation one-dimensionally using the method of separation of variables.

Julius, Leizeronok and Cukurel [18] investigated heterogeneous dual-phase lag heat transfer in different cases. They investigated the problem of one-dimensional DPL heat transfer under variable heat source in the various types of boundary conditions using the finite integral conversion technique. Asgari and Akhlaghi [19] presented a two-dimensional solution of Fourier heat transfer in a hollow cylinder made of functional graded material. The obtained equations were solved numerically by Crank-Nicholson finite difference method to determine the properties of the functional material according to the power law. Wu-xiang [20] solved a stable 3D three-dimensional circular plane of FGM. Functional properties are assumed to be a function of the thickness of the plane. He used the numerical method of the Peano-Baker series to solve his equation.

Zhang, Chen and Li [21] studied the DPL non-Fourier thermal conduction pulsed laser for the thermotherapy of skin diseases. They used 3 levels finite deference method to characterize non-Fourier heat conduction by focusing on the thermal lag during the interaction of pulsed laser with biological tissues. They showed lagging behavior of tissue and the lag later appears about 2.8 times the pulses when τ_q is equal to the pulse duration. Amiri Delouei et al [22] presented an exact analytical solution of steady-state heat conduction for the special case of a functionally graded (FG) cylindrical sector. They considered the material properties by the power-law function. Yaghoobi and Ghannad [23] present thermal studies in

cylinders of differing thickness made of FGMs with non-uniform heat fluxes in their inner and outer layers. They showed that the heterogeneity has a magnificent effect on the temperature field and thermal strain inside FG cylinders.

According to the aforementioned literature, it is found that there is no multidimensional analytical solution to the hyperbolic heat conduction equation and the DPL in a FG cylinder. Due to the efficiency of nuclear fuel pods and laser therapy of medical tumors and other cylindrical components, it is necessary to establish a basis for an accurate analytical solution of the complex mathematical heat conduction equations. The originality of this paper is that it provides the analytical solution of the two-dimensional dual phase lag non-Fourier heat conduction in Cylindrical coordinates with the functional graded material and an exact solution was obtained for different boundary conditions at the axial heat flux. In addition, The analytical approach discussed here will serve as the best comparison and validation point for other numerical and semi-analytical solutions.

2. Physical model and complex mathematical formulation

2.1 Analytical solution

A solid cylinder of functional graded material is assumed to have an axial heat flux as shown in Figure 1.

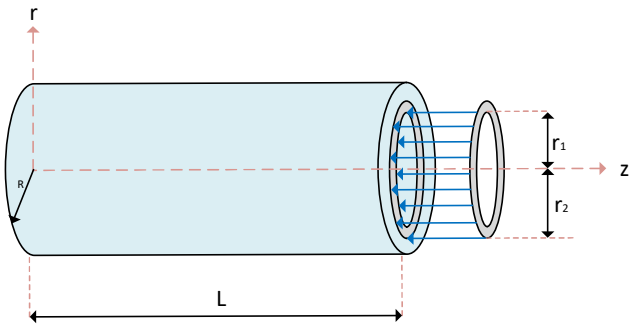

Fig. 1: solid cylinder of FGM with an axial heat flux

Assuming that the heat transfer coefficient of specific heat (C), thermal conductivity (K) and density (ρ) are variable, the governing heat transfer equation is expressed as Eq. (1).

$$\rho_r c_r \left(\frac{\partial T}{\partial t} + \tau_q \frac{\partial^2 T}{\partial t^2}\right) = \frac{1}{r}\frac{\partial}{\partial r}\left(K_r\, r \frac{\partial T}{\partial r}\right) + K_r \frac{\partial^2 T}{\partial z^2} + \tau_T \frac{\partial}{\partial t}\left(\frac{1}{r}\frac{\partial}{\partial r}\left(K_r\, r \frac{\partial T}{\partial r}\right) + K_r \frac{\partial^2 T}{\partial z^2}\right) \quad (1)$$

In which, C, K and ρ are the conduction heat transfer coefficient, specific heat and density respectively. τ_T is temperature gradient's time lag and τ_q is also heat flux's time lag.

The boundary conditions are shown in Eq. (2).

$$\begin{cases} \frac{\partial T(0.z.t)}{\partial r} = 0 \\ T(R.z.t) = T_\infty \\ T(r.0.t) = T_\infty \\ K\frac{\partial T(r.L.t)}{\partial z} = \begin{cases} 0 & r < r_1 \\ q & r_1 < r < r_2 \\ 0 & r > r_2 \end{cases} \end{cases} \quad (2)$$

The initial conditions are written as in Eq. (3).

$$I.c\begin{cases}T(r.z.0)=T_\infty\\ \frac{\partial T}{\partial t}(r.z.0)=0\end{cases} \tag{3}$$

The dimensionless parameters are obtained as shown in Eq. (4).

$$\xi=\frac{r}{R};\ Fo=\frac{\alpha_0 t}{L^2};\ \theta=K\frac{T-T_\infty}{Lq_0};\ \alpha_0=\frac{K_0}{\rho_0 c_0};\omega=\frac{z}{L};\ Ve_T=\sqrt{\frac{\alpha_0\tau_T}{L^2}};\ Ve_q=\sqrt{\frac{\alpha_0\tau_q}{L^2}};\ M=\frac{L}{R} \tag{4}$$

To assume the inhomogeneity of the cylindrical shaped material, the parameters of the FGM are assumed to be a function of the exponential radius of the cylinder.

$$K=K_0e^{\beta r}.\quad \rho=\rho_0e^{\beta r}.\quad c=c_0e^{\beta r} \tag{5}$$

By applying the parameters of the FGM in Eq. (1), the two-dimensional heat transfer equation with DPL is calculated, as shown in Eq. (6)

$$\rho_0c_0e^{2\beta r}\left(\frac{\partial T}{\partial t}+\tau_q\frac{\partial^2T}{\partial t^2}\right)=K_0e^{\beta r}\left[\frac{\partial^2T}{\partial r^2}+\left(\beta+\frac{1}{r}\right)\frac{\partial T}{\partial r}+\frac{\partial^2T}{\partial z^2}+\tau_T\frac{\partial}{\partial t}\left(\frac{\partial^2T}{\partial r^2}+\left(\beta+\frac{1}{r}\right)\frac{\partial T}{\partial r}+\frac{\partial^2T}{\partial z^2}\right)\right] \tag{6}$$

By applying dimensionless parameters in Eq. (6) and the initial and boundary conditions, thus the dimensionless DPL heat transfer equation in the FGM cylinder is calculated, as shown in Eq. (7).

$$e^{\beta R\xi}\left(\frac{\partial\theta}{\partial Fo}+{Ve_q}^2\frac{\partial^2\theta}{\partial Fo^2}\right)=M^2\frac{\partial^2\theta}{\partial\xi^2}+(\beta R\xi+1)\frac{M^2}{\xi}\frac{\partial\theta}{\partial\xi}+\frac{\partial^2\theta}{\partial\omega^2}+{Ve_T}^2\frac{\partial}{\partial Fo}\left(M^2\frac{\partial^2\theta}{\partial\xi^2}+(\beta R\xi+1)\frac{M^2}{\xi}\frac{\partial\theta}{\partial\xi}+\frac{\partial^2\theta}{\partial\omega^2}\right) \tag{7}$$

And dimensionless boundary conditions are in Eq. (8).

$$\begin{cases}\frac{\partial\theta(0.\omega.Fo)}{\partial\xi}=0\\ \theta(1.\omega.Fo)=0\\ \theta(\xi.0.Fo)=0\\ \frac{\partial\theta(\xi.1.Fo)}{\partial\omega}=\begin{cases}0 & \xi<\xi_1\\ 1 & \xi_1<\xi<\xi_2\\ 0 & \xi>\xi_2\end{cases}\end{cases} \tag{8}$$

And dimensionless initial conditions are rewritten as shown in Eq. (9).

$$I.c\begin{cases}\theta(\xi.\omega.0)=0\\ \frac{\partial\theta}{\partial Fo}(\xi.\omega.0)=0\end{cases} \tag{9}$$

The solution of Eq. (7) is divided as the sum of solving steady and transient problems and is as follows:

$$\theta(\xi.\omega.Fo)=\psi(\xi.\omega.Fo)+\phi(\xi.\omega) \tag{10}$$

Where $\phi(\xi.\omega)$ is the steady state's solution with heterogeneous boundary conditions and $\psi(\xi.\omega.Fo)$ is the transient problem's solution with homogeneous boundary conditions.

By setting the time terms to zero, the steady state equation is obtained, as shown in Eq. (11).

$$M^2\frac{\partial^2\theta}{\partial\xi^2}+(\beta R\xi+1)\frac{M^2}{\xi}\frac{\partial\theta}{\partial\xi}+\frac{\partial^2\theta}{\partial\omega^2}=0 \tag{11}$$

And corresponding boundary conditions are as equation (12)

$$\begin{cases} \frac{\partial \phi(0.\omega)}{\partial \xi} = 0 \\ \phi(1.\omega)=0 \\ \phi(\xi.0)=0 \\ \frac{\partial \phi(\xi.1)}{\partial \omega} = \begin{cases} 0 & \xi < \xi_1 \\ 1 & \xi_1 < \xi < \xi_2 \\ 0 & \xi > \xi_2 \end{cases} \end{cases} \quad (12)$$

Eq. (11) can be written as follows using the method of separation of variables.

$$\phi(\xi.\omega) = X(\xi)Z(\omega) \quad (13)$$

By applying relation (13) in Eq. (11), therefore Eq. (14) is calculated as follows.

$$\frac{M^2}{X}\left(\frac{\partial^2 X}{\partial \xi^2} + (\beta R\xi + 1)\frac{1}{\xi}\frac{\partial X}{\partial \xi}\right) = -\frac{1}{Z}\frac{\partial^2 Z}{\partial \omega^2} = -\gamma^2 \quad (14)$$

The ξ direction's equation is obtained by separating Eq. (14) as follows.

$$\xi^2 \frac{\partial^2 X}{\partial \xi^2} + (\beta R\xi + 1)\xi \frac{\partial X}{\partial \xi} + \xi^2 \frac{\gamma^2}{M^2} X = 0 \quad (15)$$

In addition, its boundary conditions are shown in Eq. (16).

$$B.c \begin{cases} \frac{\partial X(0)}{\partial \xi} = 0 \\ X(1) = 0 \end{cases} \quad (16)$$

The solution of Eq. (16) corresponding to Eq. (15) is equivalent to the Eq. (17).

$$X(\xi) = \xi^{\frac{-\beta R\xi}{2}} C_1 J_{\mathrm{A}}\left(\frac{\gamma}{M}\xi\right) + C_2 Y_{\mathrm{A}}\left(\frac{\gamma}{M}\xi\right) ; \quad A = \sqrt{\left(\frac{-\beta R\xi}{2}\right)^2} \quad (17)$$

By applying the boundary condition Eq. (16) and the solid cylinder, $Y_{\mathrm{A}}\left(\frac{\gamma}{M}\xi\right) = 0$ and the Eq. (17) is reduced as Eq. (18).

$$X(\xi) = \xi^{\frac{-\beta R\xi}{2}} C_1 J_A\left(\frac{\gamma}{M}\xi\right) \quad (18)$$

In Equation (18), $\frac{\gamma}{M}$ is the answer to Equation $J_{\mathrm{A}}\left(\frac{\gamma}{M}\right) = 0$.

The equation in the ω direction is shown in Eq. (19)

$$\frac{\partial^2 Z}{\partial \omega^2} - \gamma^2 Z = 0 \quad (19)$$

and its boundary conditions are as shown in Eq. (20).

$$B.c \quad Z(0) = 0 \quad (20)$$

The solution of the second-order differential Eq. (19) is equivalent to Eq. (21).

$$Z(\omega) = C_1 sinh(\gamma\omega) + C_2 cosh(\gamma\omega) \quad (21)$$

By applying Eq. (20), the solution of Eq. (21) is reduced to or equivalent to Eq. (22).

$$Z(\omega) = Csinh(\gamma\omega) \tag{22}$$

The general solution of the steady state Eq. (11) is calculated as shown in Eq. (23).

$$\phi(\xi.\omega) = \sum_{n=1}^{\infty} a_n \, \xi^{\frac{-\beta R\xi}{2}} sinh(\gamma_n\omega) J_{\mathrm{A}}\left(\frac{\gamma_n}{M}\xi\right) \tag{23}$$

Using the orthogonal function as well as the boundary conditions of Eq. (12), $a_n$is obtained as follows.

$$a_n = \frac{\int_{\xi_1}^{\xi_2} \xi J_{\mathrm{A}}\left(\frac{\gamma_n}{M}\xi\right) d\xi}{\gamma_n \cosh\gamma_n \int_0^1 \xi^{\frac{2-\beta R\xi}{2}} {J^2}_{\mathrm{A}}\left(\frac{\gamma_n}{M}\xi\right) d\xi} \tag{24}$$

The equation of the transient problem is shown in Eq. (25).

$$e^{\beta R\xi}\left(\frac{\partial\theta}{\partial Fo} + {Ve_q}^2 \frac{\partial^2\theta}{\partial Fo^2}\right) = M^2 \frac{\partial^2\theta}{\partial\xi^2} + (\beta R\xi + 1)\frac{M^2}{\xi}\frac{\partial\theta}{\partial\xi} + \frac{\partial^2\theta}{\partial\omega^2} + {Ve_T}^2 \frac{\partial}{\partial Fo}\left(M^2 \frac{\partial^2\theta}{\partial\xi^2} + (\beta R\xi + 1)\frac{M^2}{\xi}\frac{\partial\theta}{\partial\xi} + \frac{\partial^2\theta}{\partial\omega^2}\right) \tag{25}$$

Its corresponding boundary conditions are shown in Eq. (26).

$$\begin{cases} \frac{\partial\psi(0.\omega.Fo)}{\partial\xi} = 0 \\ \psi(1.\omega.Fo)=0 \\ \psi(\xi.0.Fo)=0 \\ \frac{\partial\psi(\xi.1.Fo)}{\partial\omega} = \begin{cases} 0 & \xi < \xi_1 \\ 1 & \xi_1 < \xi < \xi_2 \\ 0 & \xi > \xi_2 \end{cases} \end{cases} \tag{26}$$

Moreover, the initial conditions have been rewritten as follows such as Eq. (10) into the Eq. (9) are written as shown in Eq. (27).

$$I.c \begin{cases} \psi(\xi.\omega.0) = -\phi(\xi.\omega) \\ \frac{\partial\psi}{\partial Fo}(\xi.\omega.0) = 0 \end{cases} \tag{27}$$

The response of the Eq. (25) with the method of separation of variables is considered as follows:

$$\psi(\xi.\omega.Fo) = X(\xi)Z(\omega)\tau(Fo) \tag{28}$$

By applying relation of Eq. (28) to Eq. (25), following combined solution is obtained.

$$\frac{1}{\tau}\frac{\partial\tau}{\partial Fo} + \frac{{Ve_q}^2}{\tau}\frac{\partial^2\tau}{\partial Fo^2} - \frac{{Ve_T}^2}{\tau}\frac{\partial\tau}{\partial Fo}\left(\frac{1}{Xe^{\beta R\xi}}\left(M^2\frac{\partial^2 X}{\partial\xi^2} + (\beta R\xi + 1)\frac{M^2}{\xi}\frac{\partial X}{\partial\xi}\right) + \frac{1}{Ze^{\beta R\xi}}\left(\frac{\partial^2 Z}{\partial\omega^2}\right)\right) = \frac{1}{Xe^{\beta R\xi}}\left(M^2\frac{\partial^2 X}{\partial\xi^2} + (\beta R\xi + 1)\frac{M^2}{\xi}\frac{\partial X}{\partial\xi}\right) + \frac{1}{Ze^{\beta R\xi}}\left(\frac{\partial^2 Z}{\partial\omega^2}\right) == -\upsilon^2 \tag{29}$$

The ξ and ω direction's equations are obtained by separating Eq. (29) as,

$$\frac{1}{Xe^{\beta R\xi}}\left(M^2\frac{\partial^2 X}{\partial\xi^2} + (\beta R\xi + 1)\frac{M^2}{\xi}\frac{\partial X}{\partial\xi}\right) + \upsilon^2 = \frac{-1}{Ze^{\beta R\xi}}\left(\frac{\partial^2 Z}{\partial\omega^2}\right) = \eta^2 \Longrightarrow$$

$$\begin{cases} M^2\frac{\partial^2 X}{\partial \xi^2}+(\beta R\xi+1)\frac{M^2}{\xi}\frac{\partial X}{\partial \xi}+e^{\beta R\xi}(\upsilon^2-\eta^2)X=0 \\ \frac{\partial^2 Z}{\partial \omega^2}+e^{\beta R\xi}\eta^2 Z=0 \\ {Ve_q}^2\frac{\partial^2 \tau}{\partial Fo^2}+\frac{\partial \tau}{\partial Fo}\left(1+{Ve_T}^2\upsilon^2\right)\frac{\partial \tau}{\partial Fo}+\upsilon^2\tau=0 \end{cases} \quad (30)$$

Considering the equation for direction ξ and its corresponding boundary conditions, the following relation is obtained.

$$\xi^2\frac{\partial^2 X}{\partial \xi^2}+(\beta R\xi+1)\xi\frac{\partial X}{\partial \xi}+\xi^2 e^{\beta R\xi}\frac{(\upsilon^2-\eta^2)}{M^2}X=0 \quad (31)$$

$$B.c\begin{cases}\frac{\partial X(0)}{\partial \xi}=0 \\ X(1)=0\end{cases} \quad (32)$$

The answer corresponding to Eq. (31) is equivalent to the Eq. (33).

$$X(\xi)=\xi^{\frac{-\beta R\xi}{2}}C_1 J_{\mathrm{A}}\left(\frac{\sqrt{(\upsilon^2-\eta^2)e^{\beta R\xi}}}{M}\xi\right)+C_2 Y_{\mathrm{A}}\left(\frac{\sqrt{(\upsilon^2-\eta^2)e^{\beta R\xi}}}{M}\xi\right);\quad A=\sqrt{\left(\frac{-\beta R\xi}{2}\right)^2} \quad (33)$$

Given the solidity of the cylinder $Y_{\mathrm{A}}\left(\frac{\sqrt{\upsilon^2-\eta^2 e^{\beta R\xi}}}{M}\xi\right)=0$, the answer to Eq. (33) is as follows.

$$X(\xi)=\xi^{\frac{-\beta R}{2}}C_1 J_{\mathrm{A}}\left(\frac{\sqrt{(\upsilon^2-\eta^2)e^{\beta R\xi}}}{M}\xi\right) \quad (34)$$

The equation in the direction of ω can be written as Eq. (35).

$$\frac{\partial^2 Z}{\partial \omega^2}+e^{\beta R\xi}\eta^2 Z=0 \quad (35)$$

And its boundary conditions are,

$$Z(0)=0 \quad (36)$$

The answer of the Eq. (35) can now be written as in Eq. (37).

$$Z(\omega)=C_1 sin\left(\sqrt{e^{\beta R\xi}}\eta_g\omega\right)+C_2 cos(\sqrt{e^{\beta R\xi}}\eta_g\omega) \quad (37)$$

By applying the boundary conditions, the Eq. (37) is calculated as Eq. (38).

$$Z(\omega)=Asin\left(\sqrt{e^{\beta R\xi}}\eta_g\omega\right) \quad (38)$$

In equations (34) and (38), $\frac{\gamma}{M}$ and λ are the answers of equations $J_0\left(\frac{\gamma}{M}\right)=0$ and cos(λ)=0, respectively. the dimensionless time Fo's equation is indicated in Eq. (39).

$${Ve_q}^2\frac{\partial^2 \tau}{\partial Fo^2}+\frac{\partial \tau}{\partial Fo}\left(1+{Ve_T}^2\upsilon^2\right)\frac{\partial \tau}{\partial Fo}+\upsilon^2\tau=0 \quad (39)$$

Whereas, the initial condition is shown in Eq. (40).

$$\frac{\partial \tau}{\partial Fo}(0) = 0 \tag{40}$$

The answer of Eq. (39) is divided into two parts, complex and real, based on the existing conditions.

If $\left(1 + {Ve_T}^2 v^2\right)^2 - 4v^2 {Ve_q}^2 > 0$, Eq. (39) has the following real answer as follows:

$$\tau_{f.g}(t) = e^{-\frac{\left(1+{Ve_T}^2 v^2\right)Fo}{2{Ve_q}^2}} \left(C_1 sinh\left(A_{fg}\frac{Fo}{2{Ve_q}^2}\right) + C_2 \cosh\left(A_{fg}\frac{Fo}{2{Ve_q}^2}\right)\right) \tag{41}$$

If$\left(1 + {Ve_T}^2 v^2\right)^2 - 4v^2 {Ve_q}^2 < 0$, Eq. (39) has an imaginary answer as follows:

$$\tau_{f.g}(t) = e^{-\frac{\left(1+{V\ _T}^2 v^2\right)Fo}{2{Ve_q}^2}} (C_1 sin\left(\left(A_{fg}\right)_i \frac{Fo}{2{Ve_q}^2}\right) + C_2 cos(\left(A_{fg}\right)_i \frac{Fo}{2{Ve_q}^2})) \tag{42}$$

Where C_1 and C_2 are constant coefficients obtained from the initial condition (40). The value of $A_{fg}$is equal to:

$$A_{fg} = \sqrt{\left(1 + {Ve_T}^2 v^2\right)^2 - 4{Ve_q}^2 v^2}; \quad A_{fg} = i\left(A_{fg}\right)_i \tag{43}$$

The general answer of Eq. (39) is equivalent to Eq. (44).

$$\tau_{f.g}(t) = C \begin{cases} e^{-\frac{\left(1+{V\ _T}^2 v^2\right)Fo}{2{Ve_q}^2}} \left[\frac{\left(1+{Ve_T}^2 v^2\right)}{A_{fg}} \sinh\left(A_{fg}\ \frac{Fo}{2{Ve_q}^2}\right) + \cosh\left(\ A_{fg}\frac{Fo}{2{Ve_q}^2}\right)\right] \\ e^{-\frac{\left(1+{Ve_T}^2 v^2\right)\xi}{2{Ve_q}^2}} \left[\frac{\left(1+{Ve_T}^2 v^2\right)}{\left(A_{fg}\right)_i} \sin\left(\left(A_{fg}\right)_i\ \frac{Fo}{2{Ve_q}^2}\right) + \cos\left(\ \left(A_{fg}\right)_i \frac{Fo}{2{Ve_q}^2}\right)\right] \end{cases} \tag{44}$$

The transient solution of Eq. (29) is obtained by pasting the solutions in relations (34), (38) and (44) into relation (28), as follows:

$$\psi(\eta.\omega.\xi) = \sum_{f=1}^{F}\sum_{g=0}^{G} C_{fg}\,\xi^{\frac{-\beta R\xi}{2}} e^{-\frac{\left(1+{Ve_T}^2 v^2\right)Fo}{2{Ve_q}^2}} \left[\frac{\left(1+{Ve_T}^2 v^2\right)}{A_{fg}} \sinh\left(A_{fg}\ \frac{Fo}{2{Ve_q}^2}\right) + \cosh\left(\ A_{fg}\frac{Fo}{2{Ve_q}^2}\right)\right] \times$$
$$sin\left(\sqrt{e^{\beta R\xi}}\eta_g\omega\right) J_{\mathrm{A}}\left(\frac{\sqrt{(v^2-\eta^2)e^{\beta R\xi}}}{M}\xi\right) + \sum_{f=F+1}^{\infty}\sum_{g=G+1}^{\infty} C_{fg}\,\xi^{\frac{-\beta R\xi}{2}} e^{-\frac{\left(1+{Ve_T}^2 v^2\right)\xi}{2V\ _q{}^2}} \times$$
$$\left[\frac{\left(1+{Ve_T}^2 v^2\right)}{\left(A_{fg}\right)_i} \sin\left(\left(A_{fg}\right)_i\ \frac{Fo}{2{Ve_q}^2}\right) + \cos\left(\ \left(A_{fg}\right)_i \frac{Fo}{2V\ _q{}^2}\right)\right] \times sin\left(\sqrt{e^{\beta R\xi}}\eta_g\omega\right) J_{\mathrm{A}}\left(\frac{\sqrt{(v^2-\eta^2)e^{\beta R\xi}}}{M}\xi\right) \tag{45}$$

Using the boundary condition (26) and the orthogonal function, C_{fg} is equivalent to Eq. (46).

$$C_{fg} = -\frac{a_f J_{\mathrm{A}}\left(\frac{\gamma_f}{M}\xi\right)\int_0^1 \sinh(\gamma_f\omega)\, sin\left(\sqrt{e^{\beta R\xi}}\eta_g\omega\right)d\omega}{J_{\mathrm{A}}\left(\frac{\sqrt{(v^2-\eta^2)e^{\beta R\xi}}}{M}\xi\right)\int_0^1 sin^2\left(\sqrt{e^{\beta R\xi}}\eta_g\omega\right)d\omega} \tag{46}$$

2.2 Numerical solution [Validation]

For validating the analytical method's results, the problem is also examined by the finite difference method. The formulation of the numerical method by finite difference is shown in equation 47.

$$e^{\beta R\xi_{i.j}}\left(\frac{\theta_{i.j}^{n+1}-\theta_{i.j}^{n}}{\Delta Fo}+{Ve_q}^2\left(\frac{\theta_{i.j}^{n+1}-2\theta_{i.j}^{n}+\theta_{i.j}^{n-1}}{\Delta Fo^2}\right)\right)=M^2\left(\frac{\theta_{i+1.j}^{n+1}-2\theta_{i.j}^{n+1}+\theta_{i-1.j}^{n+1}}{\Delta\xi^2}+\left(\beta R\xi_{i.j}+1\right)\frac{\theta_{i+1.j}^{n+1}-\theta_{i-1.j}^{n+1}}{2\xi_{i.j}\Delta\xi}\right)+$$
$$\frac{\theta_{i.j+1}^{n+1}-2\theta_{i.j}^{n+1}+\theta_{i.j-1}^{n+1}}{\Delta\omega^2}+{Ve_T}^2M^2\left(\frac{\theta_{i+1.j}^{n+1}-2\theta_{i.j}^{n+1}+\theta_{i-1.j}^{n+1}}{\Delta Fo\ \Delta\xi^2}-\frac{\theta_{i+1.j}^{n}-2\theta_{i.j}^{n}+\theta_{i-1.j}^{n}}{\Delta Fo\ \Delta\xi^2}+\left(\beta R\xi_{i.j}+1\right)\left(\frac{\theta_{i+1.j}^{n+1}-\theta_{i-1.j}^{n+1}}{2\Delta Fo\ \xi_{i.j}\Delta\xi}-\right.\right.$$
$$\left.\left.\frac{\theta_{i+1.j}^{n}-\theta_{i-1.j}^{n}}{2\Delta Fo\ \xi_{i.j}\Delta\xi}\right)\right)+{Ve_T}^2\left(\frac{\theta_{i.j+1}^{n+1}-2\theta_{i.j}^{n+1}+\theta_{i.j-1}^{n+1}}{\Delta F\ \ \Delta\omega^2}-\frac{\theta_{i.j+1}^{n}-2\theta_{i.j}^{n}+\theta_{i.j-1}^{n}}{\Delta Fo\Delta\omega^2}\right) \quad (47)$$

The equation (48) is obtained by separating the coefficients

$$\left[\frac{e^{\beta R\xi_{i.j}}}{\Delta Fo}+\frac{{Ve_q}^2e^{\beta R\xi_{i.j}}}{\Delta Fo^2}+\frac{2M^2}{\Delta\xi^2}+\frac{2}{\Delta\xi^2}+\frac{2M^2{Ve_T}^2}{\Delta Fo\Delta\xi^2}+\frac{2{Ve_T}^2}{\Delta Fo\Delta\xi^2}\right]\theta_{i.j}^{n+1}+\left[-\frac{M^2}{\Delta\xi^2}-\frac{(\beta R\xi_{i.j}+1)M^2}{2\xi_{i.j}\Delta\xi}-\frac{M^2{Ve_T}^2}{\Delta Fo\Delta\xi^2}-\right.$$
$$\left.\frac{(\beta R\xi_{i.j}+1){Ve_T}^2M^2}{2\Delta Fo\ \xi_{i.j}\Delta\xi}\right]\theta_{i+1.j}^{n+1}+\left[-\frac{M^2}{\Delta\xi^2}+\frac{(\beta R\ \ _{i.j}+1)M^2}{2\xi_{i.j}\Delta\xi}-\frac{M^2{Ve_T}^2}{\Delta Fo\Delta\xi^2}+\frac{(\beta R\xi_{i.j}+1){Ve_T}^2M^2}{2\Delta Fo\ \xi_{i.j}\Delta\xi}\right]\theta_{i-1.j}^{n+1}+\left[-\frac{1}{\Delta\omega^2}-\right.$$
$$\left.\frac{{Ve_T}^2}{\Delta Fo\Delta\omega^2}\right]\theta_{i.j+1}^{n+1}+\left[-\frac{1}{\Delta\omega^2}-\frac{{Ve_T}^2}{\Delta Fo\Delta\omega^2}\right]\theta_{i.j-1}^{n+1}=\left[\frac{e^{\beta R\xi_{i.j}}}{\Delta Fo}+\frac{2{Ve_q}^2e^{\beta R\ \ i.j}}{\Delta Fo^2}+\frac{2{Ve_T}^2M^2}{\Delta Fo\ \Delta\xi^2}+\frac{2{Ve_T}^2}{\Delta Fo\Delta\omega^2}\right]\theta_{i.j}^{n}+\left[-\frac{{Ve_T}^2M^2}{\Delta Fo\ \Delta\xi^2}-\right.$$
$$\left.\frac{{Ve_T}^2M^2(\beta R\xi_{i.j}+1)}{2\Delta Fo\ \xi_{i.j}\Delta\xi}\right]\theta_{i+1.j}^{n}+\left[-\frac{{Ve_T}^2M^2}{\Delta Fo\ \Delta\xi^2}+\frac{{Ve_T}^2M^2(\beta R\xi_{i.j}+1)}{2\Delta F\ \ \xi_{i.j}\Delta\xi}\right]\theta_{i-1.j}^{n}+\left[-\frac{{Ve_T}^2}{\Delta Fo\Delta\omega^2}\right]\theta_{i.j+1}^{n}+\left[-\frac{{Ve_T}^2}{\Delta Fo\Delta\omega^2}\right]\theta_{i.j-1}^{n}+$$
$$\left[-\frac{{Ve_q}^2}{\Delta Fo^2}\right]\theta_{i.j}^{n-1} \quad (48)$$

Equation (48)can be written as a matrix. The matrix formation is shown in equation (49)

$$[M_1][\theta]^{n+1}=[M_2][\theta]^{n}+[M_3][\theta]^{n-1} \quad (49)$$

where $[M_1]$ and $[M_2]$ are five diagonal matrices, and $[M_3]$ is a diagonal matrix. By using the inverse matrix method, the dimensionless temperature in Equation (49) can be obtained for each time step.

3. Numerical results and discussion

3.1. An effect of the heterogeneity coefficient of the material using Fourier method, Cattaneo–Vernote model and the dual phase lag.

By applying the analytical solutions, the effect of the heterogeneity coefficient of the material is analyzed using the Fourier method (as shown in Figure. 2a), the Cattaneo–Vernote model (as shown in Figure 2b), and the dual phase lag (as shown in Figure 2c). Fig 2a, shows the relationship between Fo (dimensionless Fourier number) and dimensionless temperature at β (FG parameter) of 0 and 2. It can be seen that at temperature response is lower at Fourier β =0 compared to Fourier β =2. Fig 2a, shows the results with Cattaneo–Vernote model and it can be seen that temperature response is non-linear rise and fall between Fo 1 and 1.6 but eventually maintains its steady state mode. However, the lower temperature at Fourier β =0 compared to Fourier β =2. Figure. 2c shows smoother response compared to Cattaneo-Vernote model.

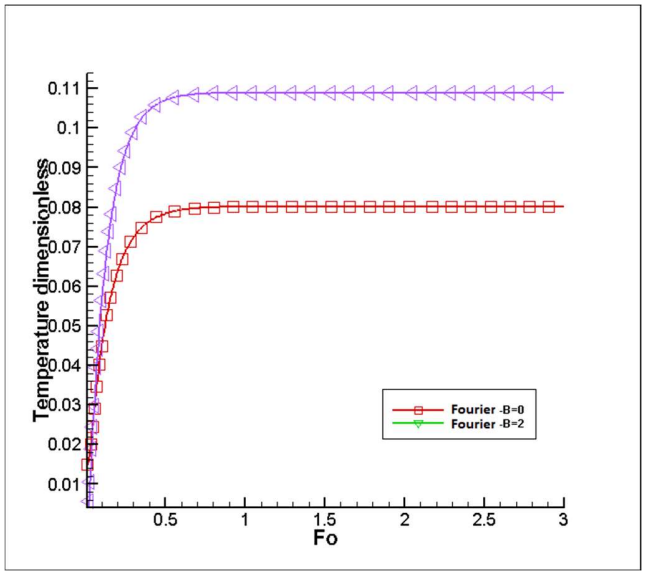

Fig. 2a. Steady temperature changes in the Fourier model

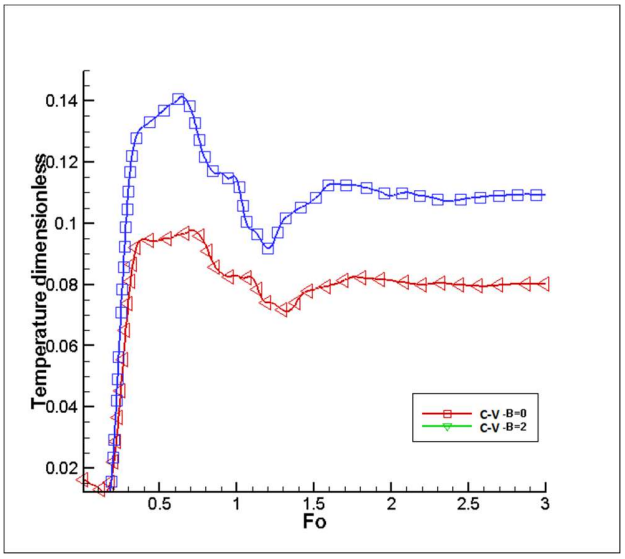

Fig. 2b. Steady temperature changes in the C-V model the Cattaneo–Vernote model.

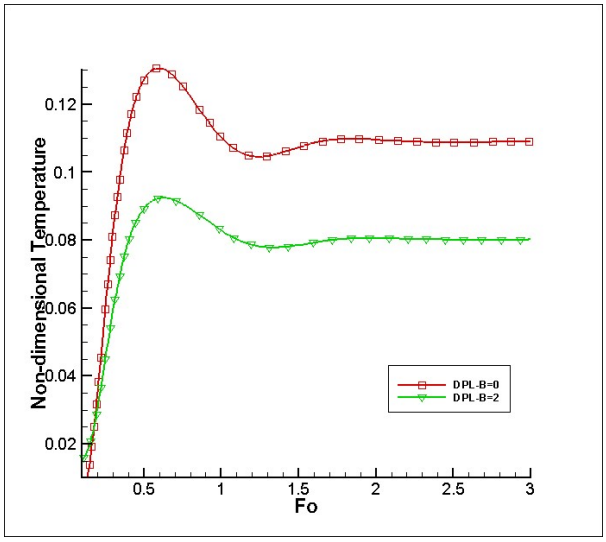

Fig. 2c. Steady temperature changes in the DPL model when

$$\xi = 0.1. \omega = 1. M = 1; Ve_q = 0.5. Ve_T = 0.2$$

3.2. An influence of non-dimensional temperature changes to the Fourier number in the pure and functional material.

Figure. 3 shows the temperature comparison of the two structures of pure matter and functional matter. Based on this, as can be seen, each model and method tends to have a constant temperature reach after Fo of 2 based on the amount of heterogeneity coefficient. It shows that one of the factors determining the amount of steady temperature is the properties of the material. Based on this, Figure. 3 is calculated according to the assumed conditions of the highest steady temperature for the pure material. It has also been observed that in the material of the FGM it takes longer to delay than in the pure material to start the heat wave in the cylinder.

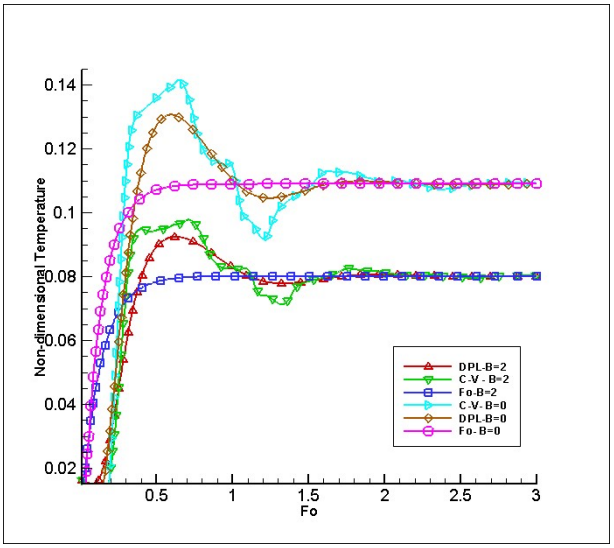

Fig. 3: Non-Dimensional temperature changes to the Fourier number in the pure matter and functional material (β = 0) and functional matter (β = 2)

3.3. Two-dimensional isotherm with applied heat flux.

Figure 4 shows a two-dimensional isotherm showing an increase of temperature. It shows that, due to the application of heat flux, the maximum temperature occurred at the point of heat flux. Figure 4a shows the amount of ripples occurs at the beginning of the heat flux, because of the initial shock of the heat wave, which disappears after a short time as shown in Figure 4b and the process of heat development progresses logically.

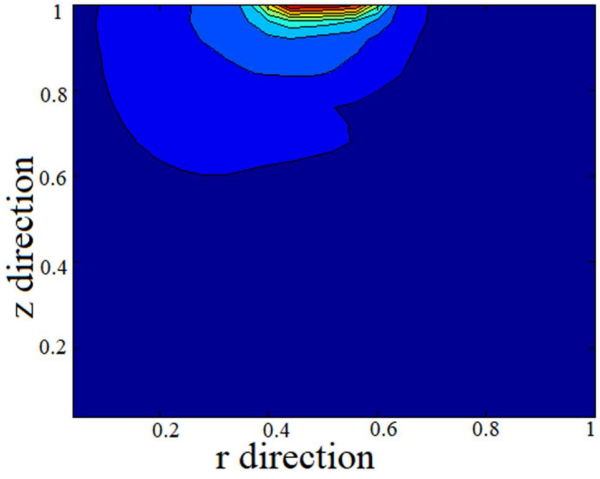

Fig. 4a. Temperature change contour at the beginning of applying heat flux

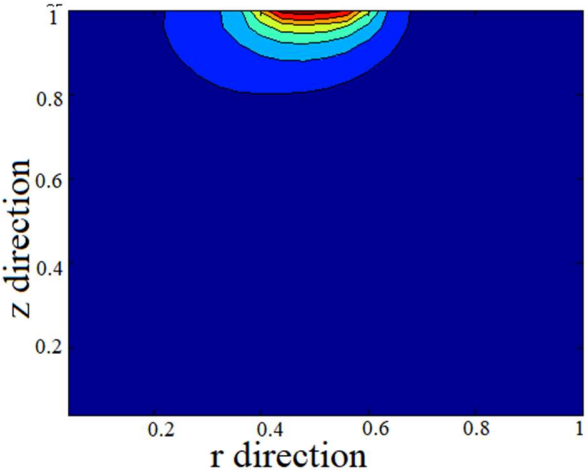

Fig. 4b. Temperature change contour after applying heat flux

3.4. An influence of increasing the dimensionless radius on non-dimensional temperature

Figure 5 shows the non-dimensional temperature changes along the dimensionless radius. In which, the maximum temperature calculated is in the range of heat flux application (0.4 and 0.6). It shows that the rate

of heat wave velocity in the pure matter is greater than the functional graded matter. This implicates that the cylindrical wall in the pure material model perceives the effect of heat flux earlier than the gross material as shown in Figure 5.

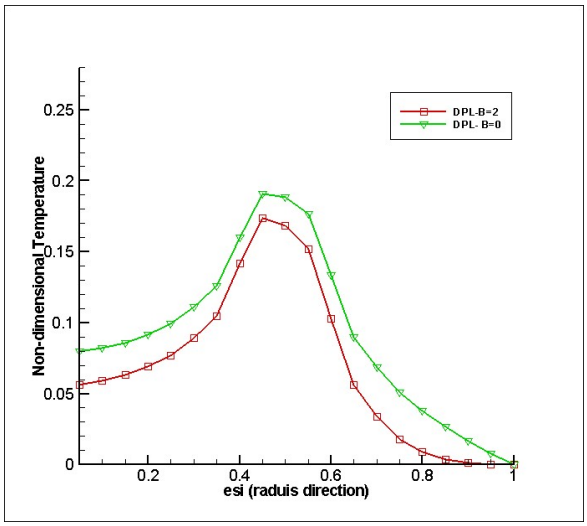

Fig. 5. Non-Dimensional temperature changes in the radius direction of the cylinder

$$fo = 0.5. \omega = 1. M = 1; Ve_q = 0.5. Ve_T = 0.2$$

Figure 6 shows the non-dimensional temperature changes along the axis of the cylinder. In which, the maximum temperature occurred at the top of the cylinder due to the application of heat flux. By comparing Figure 6 with Figure 5, the rate of heat wave in the pure material is higher than the FGM.

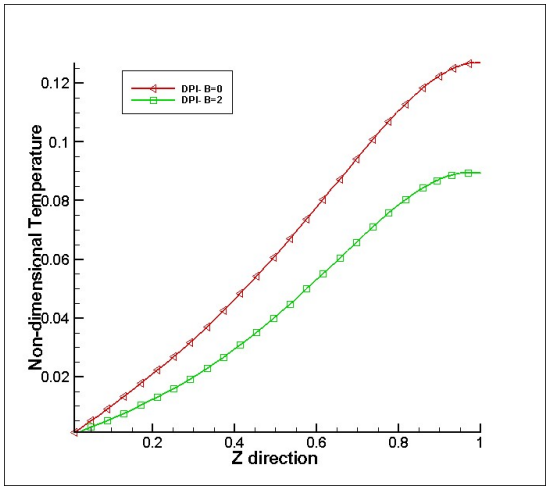

Fig. 6. Non-Dimensional temperature changes along the axis of the cylinder

$$fo = 0.5. \xi = 0.1 . M = 1; Ve_q = 0.5. Ve_T = 0.2$$

A comparison of numerical and analytical results is shown in Figure 7. The result of the number solution is obtained in mesh of $\Delta Fo = 0.01. \Delta\omega = \Delta\xi = 0.05$ values. As can be seen in Figure 7, the numerical and analytical data are consistent with each other.

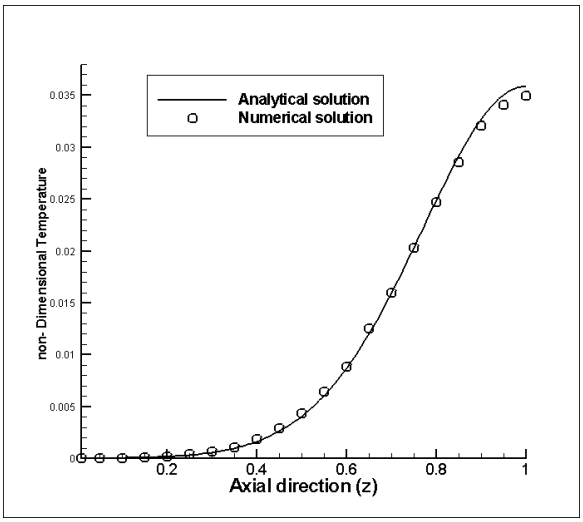

Fig. 7. Comparison of numerical solution and analytical solution

$fo = 0.2. \xi = 0\ . M = 1; Ve_q = 0.5. Ve_T = 0.2. \beta = 0.5$

4. conclusion

The Numerical thermal analyses which are based on the solution of the hyperbolic thermal conduction complex equations and the two-dimensional dual phase lag in cylindrical coordinates with the functional graded material are conducted in this study. In which a direct response for different boundary conditions in the axial heat flux is obtained. This analytical solution presented can be used as the best reference and validation base for other numerical and semi-analytical solutions. The current results provide a straightforward multivariate analytical solution of the non-Fourier conduction equation in a finite cylinder, for cylinders with any boundary conditions and, for cylinders with functional graded materials. It was found that negligible issues with the critical points being presented when compared to the Laplace operator method. In addition, with this response, the analytical solution provided can be utilized in modeling temperature profiles due to laser heating modeling on the skin and tumor, estimating the time to reach the phase change temperature and drug release in the liposome delivery system as well as stress and strain modeling and cylindrical pods with sudden and very high heat fluxes such as in the nuclear fuel sheath of a power plant.

5.References

[1] Shen, M. M.B. Bever. (1972). *Gradients in* polymeric *materials*. Journal of material science. Volume 7, Issue 7, pp 741–746.

[2] Brischetto, S. (2009). Classical and mixed multilayered plate / shell models for multi field problems analysis. Politecnico Di Torino.

[3] Wang, Liqiu, Mingtian Xu, Xuesheng Zhou. (2001). Well-posedness and solution structure of dual-phase-lagging heat conduction, Int. J. Heat and Mass Transfer 44 1659–1669.

[4] Baumeister K. J. & Hamill T. D. (1971), *Hyperbolic heat conduction equation - a solution for the seme-infinite body problem*. J. Heat Transfer 93, 126–127.

[5] Maurer M. J. & Thompson H. A. (1973*), Non-Fourier effects at high heat flux*. J. Heat Transfer 95, 284–286.

[6] Özisik M. N. & Vick B. (1984). Propagation and reflection of thermal waves in a finite medium. Int. J. Heat Mass Transfer 27, 1845–1854

[7] Moosaie, A, (2008). Axisymmetric non-Fourier temperature field in a hollow sphere. Archive of Applied Mechanics volume 79, pages679–694

[8] Barletta. A., B. Pulvirenti, (1998). Hyperbolic thermal waves in a solid cylinder with a non-stationary boundary heat flux, Int. J. Heat Mass Transfer 41 107–116.

[9] Anbarloei, Mahdi. And Elyas Shivanian. (2016). Exact Closed-Form Solution of the Nonlinear Fin Problem with Temperature-Dependent Thermal Conductivity and Heat Transfer Coefficient. Journal of Heat Transfer. ASME. Vol. 138

[10] Amiri Delouei, A. and M. Norouzi. (2015). *Exact Analytical Solution for Unsteady Heat Conduction in Fiber-Reinforced Spherical Composites Under the General Boundary Conditions*. Journal of Heat Transfer. ASME. Vol. 137.

[11] Ghasemi, Mohammad Hadi, Siamak Hoseinzadeh, Stephan Heyns, and Daniel Nicolas Wilke, (2020), Numerical Analysis of Non-Fourier Heat Transfer in a Solid Cylinder with Dual-Phase-Lag Phenomenon, Computer Modeling in Engineering and Sciences, Vol. 122, PP. 399-414.

[12] Askarizadeh, Hossein. And Hossein Ahmadikia. (2017). Extended Irreversible Thermodynamics Vs Second Law Analysis of High-Order Dual-Phase-Lag Heat Transfer. Journal of Heat Transfer. ASME. Vol. 139.

[13] Li. M, M. Lei and P.H. Wen. (2015). on-linear analysis of FGM composites by finite block method in cylindrical coordinates. Engineering structures

[14] Yang, Yu-Ching, Songhao Wang and Syun-Cheng Lin. (2016). Dual-phase-lag heat conduction in a furnace wall made of functionally graded materials. International Communications in Heat and Mass Transfer 74. PP. 76-81.

[15] C. Mishra, Subhash, and Rahul K.Chaurasia, (2015), Analysis of Dual-Phase-Lag Non-Fourier Conduction and Radiation Heat Transfer in a Planar Slab, Numerical Heat Transfer, Part A, vol. 68, Issue 9, PP. 1010-1022.

[16] Akbarzadeh, AH, and ZT Chen. (2012). Heat conduction in one-dimensional functionally graded media based on the dual-phase-lag theory. Journal of Mechanical Engineering Science

[17] Hosseini, S. M, M. Akhlaghi and M. Shakeri. (2007). Transient heat conduction in functionally graded thick hollow cylinders by analytical method. Heat Mass Transfer

[18] Julius, Simon. Boris Leizeronok and Beni Cukurel. (2018). Nonhomogeneous Dual-Phase-Lag Heat Conduction Problem: Analytical Solution and Select Case Studies. Journal of Heat Transfer. ASME. Vol. 140.

[19] Asgari, Masoud and Mehdi Akhlaghi. (2009). Transient heat conduction in two-dimensional functionally graded hollow cylinder with finite length. Heat Mass Transfer.

[20] Wu-xiang, LIU. (2013). Analysis of steady heat conduction for 3D axisymmetric functionally graded circular plate. Journal of Central South University Press.

[21] Zhang, Yong, Bin Chen and Dong Li, (2017), Non-Fourier effect of laser-mediated thermal behaviors in bio-tissues: A numerical study by the dual-phase-lag model, International Journal of Heat and Mass Transfer, Vol. 108, PP. 1428-1438.

[22] Amiri Delouei, A, A. Emamian, S. Karimnejad, H. Sajjadi, and A. Tarokh, (2019), On 2D asymmetric heat conduction in functionally graded cylindrical segments: A general exact solution, International Journal of Heat and Mass Transfer, Vol. 143, 118515, PP. 1-12.

[23] Yaghoobi, M.Parhizkar and M.Ghannad, (2020), An analytical solution for heat conduction of FGM cylinders with varying thickness subjected to non-uniform heat flux using a first-order temperature theory and perturbation technique, International Communications in Heat and Mass Transfer, Vol. 116, 104684.